Int. J. Electrochem. Sci., 15 **(2020)** 7763 – 7773, doi: 10.20964/2020.08.88

International Journal of
ELECTROCHEMICAL
SCIENCE
www.electrochemsci.org

Morphology-Controllable Synthesis of one-dimensional ZnO nanostructures on graphene oxide-based electrode and its enhanced electrochemical performance for supercapacitor application

Lihua Lin, XueLi Yao, Li Ma[*]

Department of Telecommunication and information, Xi'an University of Science and Technology, Xi'an 710054, China
[*]E-mail: mary@xust.edu.cn

Received: 2 April 2020 / *Accepted:* 24 May 2020 / *Published:* 10 July 2020

Different morphologies of vertically aligned ZnO nanostructures were synthesized onto graphene oxide (GO) coated indium thin oxide (ITO) electrode by electrochemical technique and considered for supercapacitor application. The morphology of ZnO nanowires were successfully transformed and controlled into other morphologies like nanorods, nanocones and nanopillars by changing the applied current density and growth temperature. Structural and morphological studies indicated that the as-grown ZnO nanostructures were preferentially synthesized along the c-axis direction with hexagonal wurtzite structure. Cyclic voltammetry measurements of different morphologies of ZnO based electrodes confirms that cone-shaped ZnO nanostructures exhibited high specific capacitance of 463.7 F g^{-1} at 20 mVs^{-1} scan rate, which can be mainly associated with the higher specific surface area of ZnO nanocone electrodes than those of other morphologies.

Keywords: Graphene oxide; ZnO nanoconces; Supercapacitor application; Cyclic voltammetry; Electrochemical impedance spectroscopy

1. INTRODUCTION

Compact electronics and storage of smart-grid electrochemical energy make use of supercapacitors (SCs) due to their better energy densities and power densities in comparison to electrostatic capacitors and batteries, respectively [1-3]. Some SCs are accessible in the market to prolong battery life in electronic equipment, but then again they are only in a development phase [4]. The power density of supercapacitors is lesser compared to batteries [5]. So, the development of SCs is to enhance the power density and hence lowers the price. Based on the charge storage mechanism, supercapacitors are split into electric double-layer capacitors (EDLCs) in which absorbance of charge

occurs on the electrode surface and pseudocapacitors (PCs) in which faradaic redox reactions occur near and on the surface [6, 7]. In recent times, attention has been drawn by researchers towards cost-effective high energy density electrode materials due to their better ability to recall power density [8]. A combination of EDLCs with the PCs in the SCs can bring forth better performance. In recent years, graphene has received significant attention due to its high electrical conductivity, mechanical strength and large surface area [9, 10], which have been used in different fields containing sensor, nanoelectronics and supercapacitor [11, 12]. In the past few years, graphene, a 2-dimensional nanostructure comprised of one layer carbon atoms with sp^2 bonds, have gained attention due to their superiority in almost all properties [13]. Nevertheless, regardless of their theoretical worth, graphene nanosheets face issues related to accumulation or stacking again due to the interaction of Vander Waals forces that decreases their specific surface area along with the capacitance [14]. To avert accumulation, a metal/metal oxide or a conducting polymer can be implanted in between the graphene nanosheet layers [15, 16]. Pseudocapacitive transition-metal oxides like NiO, MnO_2, and RuO_2, have been considered widely as active electrode materials for SCs due to their large charge transfer reaction and high energy density based on reversible and fast redox reactions at the surface of the electrode, subsequent in higher specific capacitance above that of carbon-based materials by electric double-layer charge storage [17-19]. However, they have drawbacks that hamper their efficiency, like their low abundance, expense, poor rate capability, inferior electrical conductivity and reversibility throughout the charge-discharge process. So, researchers had led theoretical studies and experiments to detect cost-effective substitutes. A variety of materials had been investigated not limiting to ZnO, Fe_2O_3 and TiO_2 [20, 21]. Among those materials, zinc oxide is mostly applied in solar cells, photocatalysts, sensors and Li-ion batteries due to its inertness, cheap, eco-friendly and available in plenty [22]. Hence, a combination of graphene and zinc oxide as a substitute for current-collector materials in SCs has gained much attention in research. Although the structural design of metal oxides is of great importance for the use in electrochemical devices, it is very difficult to find articles on the morphological effect of semiconductor based electrodes on their electrochemical performance, especially in SCs. In this study, a facile electrochemical approach was used to grow different morphologies of ZnO nanostructures on graphene oxide electrode to enhance its capacitive properties. Electrochemical characterizations of ZnO nanostructures as SC electrodes, as well as cyclic voltammetry and electrochemical impedance spectroscopy in 1M KOH electrolyte, expose enhanced specific capacitances of cone-shape ZnO nanostructures compared to other morphologies.

2. MATERIALS AND METHODS

The cleaned indium tin oxide glass (ITO) substrates were employed to directly deposit graphene oxide (GO) thin layer by hot filament chemical vapour deposition (HFCVD) technique, by the use of methane (CH_4) and hydrogen (H_2) gases mixture. The ITO substrate was placed into the HFCVD compartment and annealed in an H_2 atmosphere (65 sccm) for 30 min. Additional annealing was achieved by an unending supply of H_2 with a constant rate of flow, at the filament temperature of 1200 °C for 5 min to eliminate the hints of organic materials and oxide films from the ITO. At last, the methane (CH_4, 50 sccm) as a carbon source was placed into the device for 5 min to yield a thin coat of GO on the

ITO substrate and the system was let to come back to room temperature by allowing argon (Ar, 200 sccm) to flow for an hour and a half. The GO layer on ITO (GO/ITO) substrates was employed to deposit zinc oxide nanorods with vertical alignment.

The zinc oxide nanorods with vertical alignment were full-grown by the electrochemical method on GO/ITO substrate. The aqueous growth solution was made ready by mixing 25 mM of zinc nitrate hydrate ($Zn(NO_3)_2 \cdot 6H_2O$, 99.99%) and 25 mM of hexamethylenetetramine (HMT; $C_6H_{12}N_4$, 99%) in 50 ml of DI water using magnetic stirrer. In the apparatus, the GO/ITO substrate positioned as a cathode on the exterior cell wall and the Pt wire as an anode were attached to the external direct current (DC) power supply. Also, a basic thermometer was thrust into the solution, letting temperature control and measurements. The development of zinc oxide nanostructures was done with the current density ranging from 0.1 to 1 $mAcm^{-2}$ at 70 °C (and 90 °C) for 60 min [23]. Subsequent the growth of ZnO nanostructures, they were cleansed with DI water and dehydrated using a flow of N_2 gas.

The phase and crystallinity of the nanostructures were determined using an X-ray diffractometer (Seifert, Model 3003 TT) in the range of $2\theta=10°–70°$ and CuKα radiation ($\lambda=0.154$ 06 nm). Field-emission scanning electron microscopy (FESEM; Carl ZEISS EVOMA 15) was used to characterize the surface morphology of the electrodes. Electrochemical impedance spectroscopy (EIS) was employed to examine the charge transfer with a potential of 10 mV at frequencies ranging from 0.1 Hz to 0.1MHz. The as-fabricated device is lightweight with a total mass of ~8 mg for the electrode materials. Cyclic voltammetry (CV) measurements were done in –0.1 to 1 V potential range with mass loading of 8.5 mg/cm^2 at a 30 mVs^{-1} scan rate in a 1M KOH aqueous electrolyte.

3. RESULTS AND DISCUSSION

The development environments had influenced the exterior of the zinc oxide nanorods to have various structures of the zinc oxide nanorods. Figure 1 displays surface FESEM images of ZnO nanorods deposited on the GO/ITO substrate without seed layer under different conditions. The GO sheets were formed and consistently organized on the ITO substrate with the GO thickness of ~500 nm. The exterior images display that zinc oxide nanorods are extremely thick and developed in vertical alignment on GO/ITO substrates and have hexagonal morphology. As shown in Fig. 1a, the ZnO nanowires are grown electrochemically under exerted current density of 0.1 mA $mAcm^{-2}$ at 70 °C designates a narrow diameter allocation with a mean diameter of ~38 nm and the length of below 600 nm.

The ZnO nanorods prepared at the similar state but then at an inflated temperature (90 °C) exhibited a wide diameter allocation and had a consistently wide length size (approximately 800 nm) with a flawless hexagonal form and ultra-flat exteriors (Fig. 1b). The mean diameter of the zinc oxide nanorods slowly enhanced from 38 nm to 95 nm with an increase in temperature from 70 °C to 90 °C.

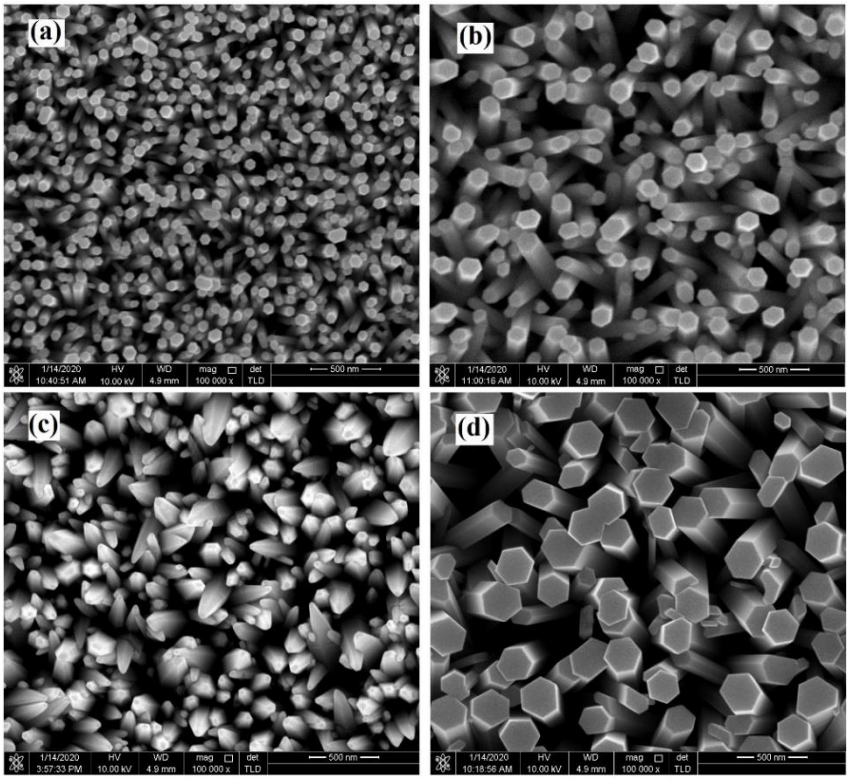

Figure 1. FESEM images of ZnO nanostructures grown on GO/ITO substrate at various growth conditions (a) 0.1 $mAcm^{-2}$ current density and 70 °C growth temperature (b) 0.1 $mAcm^{-2}$ current density and 90 °C growth temperature (c) 0.5 $mAcm^{-2}$ current density and 70 °C growth temperature (d) 1 $mAcm^{-2}$ current density and 90 °C growth temperature.

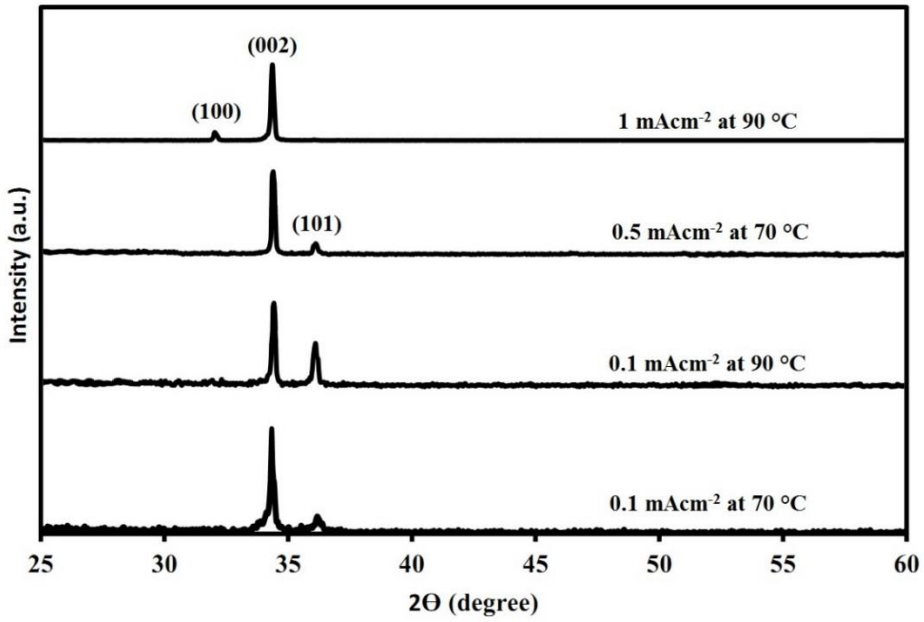

Figure 2. XRD spectra of the ZnO nanostructures with different morphologies

At the current density of 0.5 $mAcm^{-2}$ and 70 °C, a nanocone (NC)-like structure is acquired over the entire ITO (Fig. 1c). Figure 1c shows that the altitude of the oriented zinc oxide nanostructures was

enlarged by nearly 1.7 μm. The separate zinc oxide NCs were aggregated nearby the ITO as of quick sideway proportion of growth. As the altitude of the zinc oxide nanorods was enlarged, the converted electric field intensity became weak due to their high resistivity of the zinc oxide nanorods, and the adsorption of the Zn^{2+} ions was restricted at the end of the zinc oxide NRs. Furthermore, the concentration of zinc ion was inferior to that of hydroxide$^-$ ion as the production of hydroxide ions was reinforced by HMT [24]. So, the zinc oxide NRs reduced in diameter towards the finish of the growing process.

As the current density escalated to 1 $mAcm^{-2}$ at 90 °C, the structure varies from the NCs to the nanopillar (NP) structures (figure 1d). A rise in the current density and temperature originates the zinc oxide nanorods to first diameter enlargement and then eventually to enhance the length. The average diameter and typical length of these NPs is about 320 nm and 2.2 μm, respectively.

Fig. 2 displays the XRD spectra of the as-grown zinc oxide nanorods with different morphologies synthesized by electrochemical method. The diffraction peaks were seen to be similar to the hexagon-shaped zinc oxide crystalline with a wurtzite structure (ICSD 01-080-0074). They were upright crystalline without any new phase or defects. The leading (0 0 2) peak that was seen in the XRD spectra sturdily reinforces the high notch of alignment with the c-axis perpendicular to the substrate exterior [25]. Also, the robust intensity and thin size of the ZnO diffraction peaks likewise designated that the resultant zinc oxide nanorods full-grown at 0.1 mA cm^{-2} and 70 °C had better crystalline structure than the rest.

EIS is a well-established powerful device to determine the separation and transfer of charges in various applications [26]. To examine the electrochemical performance of as-grown zinc oxide-based electrodes in the SC, the electrochemical characterizations were at first done in an electrochemical cell with a 1M potassium hydroxide aqueous electrolyte. Figure 3 indicates the impedance spectra of various electrodes fabricated. EIS measurements were done in in the frequency ranging from 1MHz to 0.01Hz with 10 mV open circuit potential to monitor the electrochemical behavior of the electrodes. The impedance results were derived from the equivalent circuit as shown in the inset of Figure 3. The EIS data can be fitted to an equivalent circuit, which consisted of a bulk solution resistance (R_s), a charge-transfer resistance (R_{ct}), and a double-layer capacitance (C_{dl}). The parameters obtained from the Nyquist plot are listed in Table 1. The GO/ITO electrode displays the semicircle with the largest radius with the 38530 Ω charge transfer resistance (R_{ct}). But the radius decreased with an increase in growth of nanorods on the GO/ITO, along with the decline in R_{ct} value showing the enhanced rate of electron transfer [27].

A shown in figure 3, the ZnO NCs /GO/ITO electrode (R_{ct} 8235Ω) displayed the highest efficiency and an enhanced rate of electron transfer compared to the other morphologies. Therefore, the ZnO NCs/GO/ITO electrode was chosen to perform additional electrochemical characterization and to be used in supercapacitor applications.

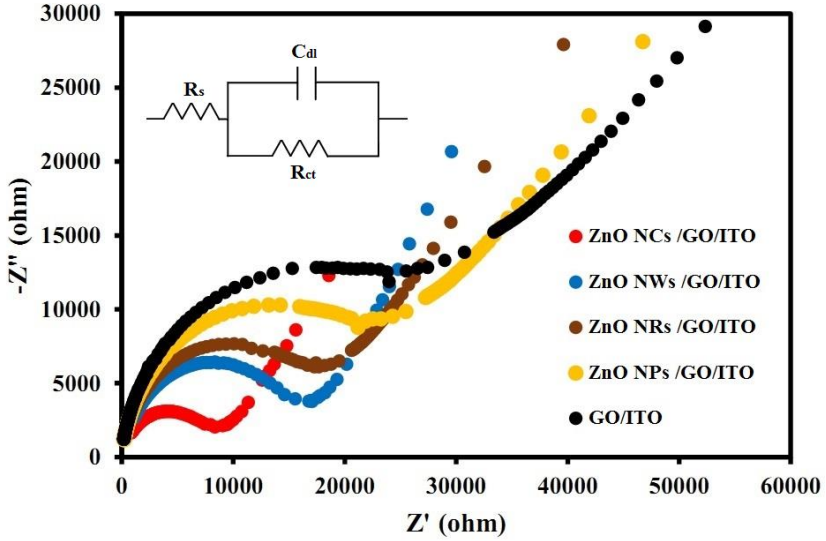

Figure 3. Impedance spectra of ZnO with different morphologies grown on GO/ITO electrodes in 1MHz to 10 mHz frequency range with 10 mV open circuit potential

Table 1. Electrochemical parameters from the fitting using the equivalent circuit in Figure 3 for various electrodes

Electrodes	R_s (Ω cm^2)	R_{ct} (kΩ cm^2)	C_{dl} (μF cm^{-2})
GO/ITO	67.8	38.530	0.25
ZnO NPs /GO/ITO	75.4	29.283	0.31
ZnO NRs /GO/ITO	64.6	22.845	0.39
ZnO NWs /GO/ITO	72.8	17.920	0.46
ZnO NCs /GO/ITO	74.3	8.235	0.88

Figure 4 illustrates the CV curves of ZnO with different morphologies grown on GO/ITO electrodes and the plain GO/ITO with 20 mVs^{-1} scan rate in a potential window ranges from 0.1 to 0.9V. The CV plots of all ZnO nanostructures show a couple of redox points at about 0.58 V and 0.72 V (versus Ag/AgCl), displaying the characteristic pseudocapacitive performance. Through the Faradaic redox process, the intercalation and deintercalation of the alkali metal K^+ happening on the electrode exterior can be characterized as trails [28]:

$$ZnO + K^+ + e^- \leftrightarrow ZnOK \qquad (1)$$

NCs displayed a higher redox peak current density in comparison with other structures. The surrounded area in the CV plot of the ZnO NC electrodes was likewise greater than that of the other electrodes, representing that zinc oxide NCs/GO/ITO own improved capacitance related to other structures [29]. Though we can similarly detect the existence of redox points in the CV plot of plain GO/ITO electrode, which can be attributed to the contaminants on the surface of the electrode, the

current density is much lesser in relation to those of zinc oxide nanostructures/GO/ITO, signifying that the capacitance involvement from the GO/ITO electrode is insignificant.

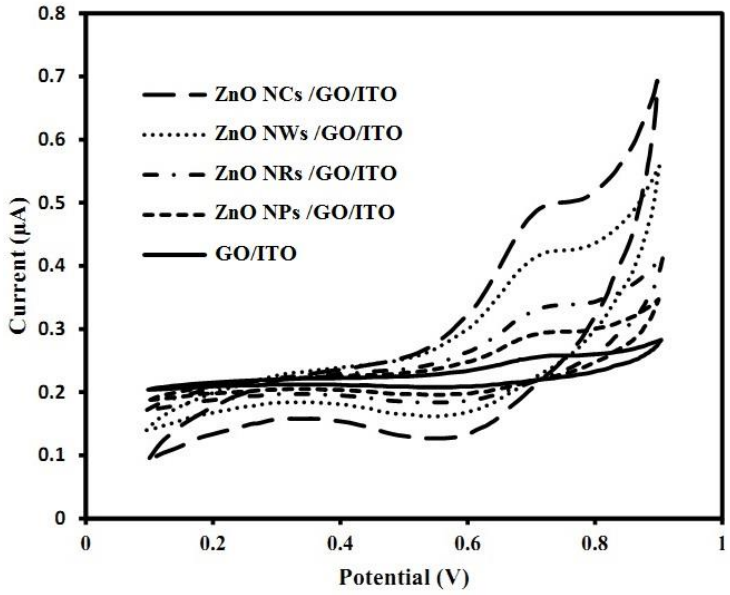

Figure 4. CV curves of ZnO with different morphologies grown on GO/ITO electrodes and the bare GO/ITO at 20 mV s^{-1} scan rate in potential from 100 to 750 mV in 1 M KOH electrolyte.

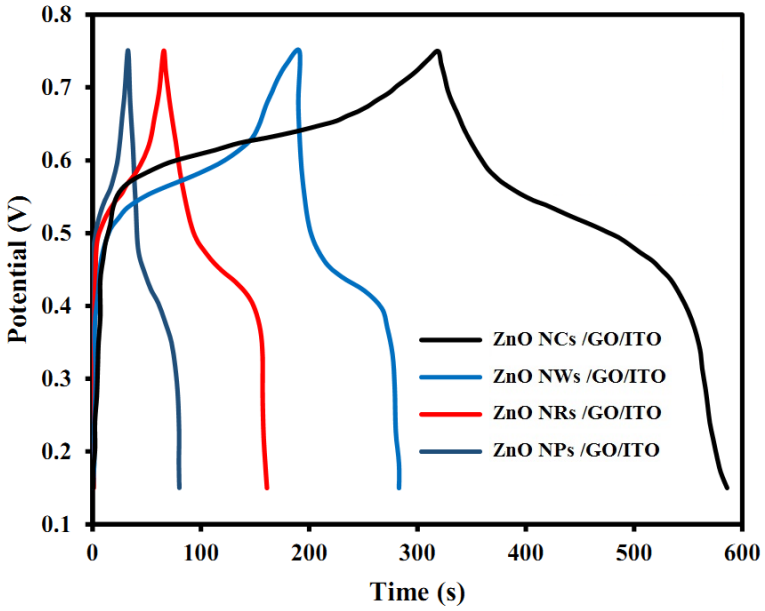

Figure 5. Galvanostatic charge–discharge curves of ZnO NC, ZnO NW, ZnO NR and ZnO NP electrodes at a current density of 0.05 mA g^{-1} in a potential window between 0.15 and 0.75 V

The galvanostatic charge–discharge measurements for both ZnO NC, ZnO NW, ZnO NR and ZnO NP electrodes were carried out to further characterize the electrochemical properties of various nanostructures. Figure 5 indicates the galvanostatic charge–discharge curves comparing ZnO NCs with those of other morphologies at a current density of 0.05 mA g^{-1} in a potential window between 0.15 and

0.75 V. The nonlinear shapes of the discharge curves was expected from the pseudocapacitance behaviour of ZnO, which is distinct from the linear triangular shape of electrical EDLCs [30]. The discharge time of the nanocone is significantly longer than the other electrodes indicating a better rate of discharge, which is in agreement with the result from the CV (figure 4).

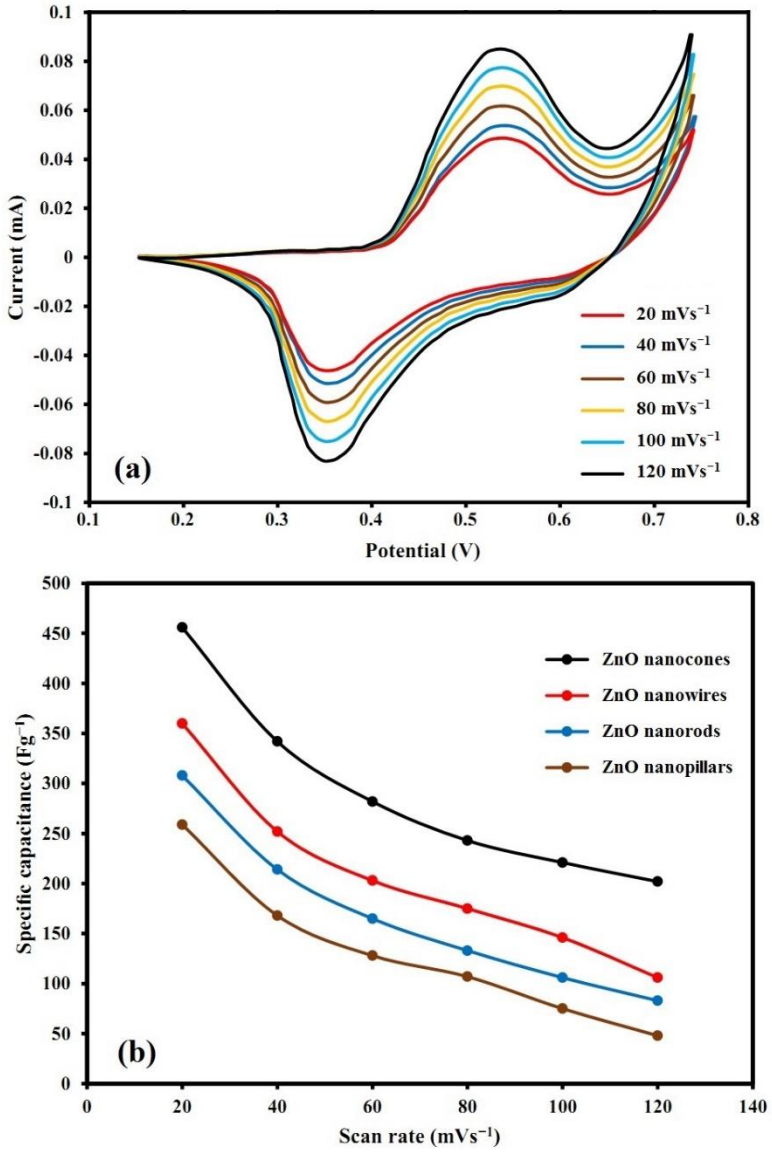

Figure 6. (a) CVs of the ZnO NCs/GO/ITO electrode at different scan rates from 20-120 mVs^{-1} in 1 M KOH electrolyte (b) The specific capacitance of ZnO with different morphologies grown on GO/ITO electrodes.

Figure 6a displays the CV graphs of the zinc oxide NCs/GO/ITO electrode at a different scan rate ranging from 20 to 120 mVs^{-1}. With the rise in the rate of the scan, the currents of the cathodic and anodic peak rose, representing an interchangeable and fast redox reaction at the electrodes. The C_m, mass-specific capacitance of these electrodes can be deduced from the CV plot using the succeeding formula [31]:

$$C_m = \frac{I}{MS(V_1 - V_2)} \int_{V_1}^{V_2} / dV \qquad (2)$$

where C_m, S, M, I, V_1, and V_2 represent the mass specific capacitance (Fg^{-1}), the scan rate (Vs^{-1}), the active material mass (g), the current (A), minor and major values of the potential range (V) in the CV plots, respectively. By using eq. 2, the C_m of all electrodes were estimated from the CV plots and graphed as a function of the rate of scan (figure 6b). The zinc oxide NCs validated a better C_m at every rate of scan. All electrodes validated improved C_m with a reduce rate of scan that was characteristic restricted rate performance of the SCs. Overall, the restricted rate performance of the electrodes was accredited to the materials with inhomogeneous porosity [32]. Figure 6b displays that the zinc oxide NCs/GO/ITO indicated a very high capacitance of 463.7 Fg^{-1} at 20 mVs^{-1}, which was more than that of other structures. Even at 120 mVs^{-1} scan rate, zinc oxide NCs still maintain C_m of 216.5 Fg^{-1}, which indicated an excellent rate capability.

4. CONCLUSIONS

One-dimensional nanostructures are alternative materials for fabricating active electrode in supercapacitors because they have outstanding thermal stability, robust adsorption/desorption capability and large specific surface area, which can assist as promoter and support to keep semiconductors with enhanced electrochemical properties. In this work, different morphologies of vertically aligned ZnO nanostructures were synthesized onto GO/ITO glass electrode by electrochemical technique and considered for supercapacitor application. The morphology of ZnO NWs were successfully transformed and controlled in to other morphologies like NRs, NCs and NPs by changing the applied current density and growth temperature. Structural and morphological studies indicated that the as-grown ZnO nanostructures were preferentially synthesized along the c-axis direction with hexagonal wurtzite structure. CV measurements of different morphologies of ZnO based electrodes confirms that cone-shaped ZnO nanostructures exhibited high specific capacitance of 463.7 Fg^{-1} at 20 mVs^{-1} scan rate, which can be mainly associated with the higher specific surface area of ZnO nanocone electrodes than those of other morphologies.

ACKNOWLEDGEMENT
This research was supported from Science and Technology Project of State Grid Xizang Electric Power Co., Ltd (SGXZJY00JHJS2000007), Influence of Energy Storage Technology Application on Power Grid and Science and Technology Project of State Grid Zizang Electric Power Co., Ltd (SGXZJY00JHJS2000008) Research Technology Service of Multi Energy Complementary Demonstration Application.

References

1. C. Zou, L. Zhang, X. Hu, Z. Wang, T. Wik and M. Pecht, *Journal of Power Sources*, 390 (2018) 286.
2. F. Wu, R. Li, L. Huang, H. Miao and X. Li, *Scientometrics*, 110 (2017) 113.
3. G. Kim, J. Kang, G. Choe and S. Yim, *International Journal of Electrochemical Science*, 12 (2017) 10015.
4. B.Y. Guan, X.Y. Yu, H.B. Wu and X.W. Lou, *Advanced materials*, 29 (2017) 1703614.
5. J. Rocabert, R. Capó-Misut, R.S. Muñoz-Aguilar, J.I. Candela and P. Rodriguez, *IEEE Transactions on Industry Applications*, 55 (2018) 1853.
6. C.-W. Liew, S. Ramesh and A. Arof, *Materials & Design*, 92 (2016) 829.
7. M. Teuber, M. Strautmann, J. Drillkens and D.U. Sauer, *ACS applied materials & interfaces*, 11 (2019) 18313.
8. K. Liang, L. Ju, S. Koul, A. Kushima and Y. Yang, *Advanced Energy Materials*, 9 (2019) 1802543.
9. H. Karimi-Maleh and O.A. Arotiba, *Journal of colloid and interface science*, 560 (2020) 208.
10. M. Wang and Y.-X. Xu, *Chinese Chemical Letters*, 27 (2016) 1437.
11. S. Changaei, J. Zamir-Anvari, N.-S. Heydari, S.G. Zamharir, M. Arshadi, B. Bahrami, J. Rouhi and R. Karimzadeh, *Journal of Electronic Materials*, 48 (2019) 6216.
12. F. Tahernejad-Javazmi, M. Shabani-Nooshabadi and H. Karimi-Maleh, *Composites Part B: Engineering*, 172 (2019) 666.
13. J. Liu, M. Zheng, X. Shi, H. Zeng and H. Xia, *Advanced Functional Materials*, 26 (2016) 919.
14. X. He, N. Zhang, X. Shao, M. Wu, M. Yu and J. Qiu, *Chemical Engineering Journal*, 297 (2016) 121.
15. Y. Xu, X. Li, G. Hu, T. Wu, Y. Luo, L. Sun, T. Tang, J. Wen, H. Wang and M. Li, *Applied Surface Science*, 422 (2017) 847.
16. J. Li, J. Guo, X. Zhang, Y. Huang and L. Guo, *International Journal of Electrochemical Science*, 12 (2017) 1157.
17. C.-q. Yi, J.-p. Zou, H.-z. Yang and L. Xian, *Transactions of Nonferrous Metals Society of China*, 28 (2018) 1980.
18. Q. Jiang, N. Kurra, M. Alhabeb, Y. Gogotsi and H.N. Alshareef, *Advanced Energy Materials*, 8 (2018) 1703043.
19. R. Asadpour, N.B. Sapari, M.H. Isa, S. Kakooei, K.U. Orji, *Fibers and Polymers*, 16(2015) 1830.
20. G.-C. Li, P.-F. Liu, R. Liu, M. Liu, K. Tao, S.-R. Zhu, M.-K. Wu, F.-Y. Yi and L. Han, *Dalton Transactions*, 45 (2016) 13311.
21. R. Dalvand, S. Mahmud and J. Rouhi, *Materials Letters*, 160 (2015) 444.
22. J. Rouhi, C.R. Ooi, S. Mahmud and M.R. Mahmood, *Electronic Materials Letters*, 11 (2015) 957.
23. M. Alimanesh, Z. Hassan and N. Zainal, *Optical Materials*, 72 (2017) 276.
24. J. Rouhi, C.R. Ooi, S. Mahmud and M.R. Mahmood, *Materials Letters*, 147 (2015) 34.
25. F. Husairi, J. Rouhi, K. Eswar, C.R. Ooi, M. Rusop and S. Abdullah, *Sensors and Actuators A: Physical*, 236 (2015) 11.
26. M.F.M. Noh, M.F. Soh, C.H. Teh, E.L. Lim, C.C. Yap, M.A. Ibrahim, N.A. Ludin and M.A.M. Teridi, *Solar Energy*, 158 (2017) 474.
27. F. Husairi, J. Rouhi, K. Eswar, A. Zainurul, M. Rusop and S. Abdullah, *Applied Physics A*, 116 (2014) 2119.
28. X. Dong, Y. Cao, J. Wang, M.B. Chan-Park, L. Wang, W. Huang and P. Chen, *RSC advances*, 2 (2012) 4364.
29. M. Miraki, H. Karimi-Maleh, M.A. Taher, S. Cheraghi, F. Karimi, S. Agarwal and V.K. Gupta, *Journal of Molecular Liquids*, 278 (2019) 672.

30. Ü. Alver, A. Tanrıverdi and Ö. Akgül, *Synthetic Metals*, 211 (2016) 30.
31. S. Zhang, B. Yin, H. Jiang, F. Qu, A. Umar and X. Wu, *Dalton Transactions*, 44 (2015) 2409.
32. Y. Wang, W. Lai, N. Wang, Z. Jiang, X. Wang, P. Zou, Z. Lin, H.J. Fan, F. Kang and C.-P. Wong, *Energy & Environmental Science*, 10 (2017) 941.